High Transverse Momentum Hadron Spectra at $\sqrt{s_{NN}} = 17.3\,\mathrm{GeV}$, in Pb+Pb and p+p Collisions

C. Alt,[9] T. Anticic,[23] B. Baatar,[8] D. Barna,[4] J. Bartke,[6] L. Betev,[10] H. Białkowska,[20] C. Blume,[9] B. Boimska,[20] M. Botje,[1] J. Bracinik,[3] R. Bramm,[9] P. Buncic,[10] V. Cerny,[3] P. Christakoglou,[2] P. Chung,[19] O. Chvala,[14] J.G. Cramer,[16] P. Csató,[4] P. Dinkelaker,[9] V. Eckardt,[13] D. Flierl,[9] Z. Fodor,[4] P. Foka,[7] V. Friese,[7] J. Gál,[4] M. Gaździcki,[9,11] V. Genchev,[18] G. Georgopoulos,[2] E. Gładysz,[6] K. Grebieszkow,[22] S. Hegyi,[4] C. Höhne,[7] K. Kadija,[23] A. Karev,[13] D. Kikola,[22] M. Kliemant,[9] S. Kniege,[9] V.I. Kolesnikov,[8] E. Kornas,[6] R. Korus,[11] M. Kowalski,[6] I. Kraus,[7] M. Kreps,[3] A. Laszlo,[4,*] R. Lacey,[19] M. van Leeuwen,[1] P. Lévai,[4] L. Litov,[17] B. Lungwitz,[9] M. Makariev,[17] A.I. Malakhov,[8] M. Mateev,[17] G.L. Melkumov,[8] A. Mischke,[1] M. Mitrovski,[9] J. Molnár,[4] St. Mrówczyński,[11] V. Nicolic,[23] G. Pálla,[4] A.D. Panagiotou,[2] D. Panayotov,[17] A. Petridis,[2,†] W. Peryt,[22] M. Pikna,[3] J. Pluta,[22] D. Prindle,[16] F. Pühlhofer,[12] R. Renfordt,[9] C. Roland,[5] G. Roland,[5] M. Rybczyński,[11] A. Rybicki,[6] A. Sandoval,[7] N. Schmitz,[13] T. Schuster,[9] P. Seyboth,[13] F. Siklér,[4] B. Sitar,[3] E. Skrzypczak,[21] M. Slodkowski,[22] G. Stefanek,[11] R. Stock,[9] C. Strabel,[9] H. Ströbele,[9] T. Susa,[23] I. Szentpétery,[4] J. Sziklai,[4] M. Szuba,[22] P. Szymanski,[10,20] V. Trubnikov,[20] D. Varga,[4,10] M. Vassiliou,[2] G.I. Veres,[4,5] G. Vesztergombi,[4,4] D. Vranić,[7] A. Wetzler,[9] Z. Włodarczyk,[11] A. Wojtaszek,[11] I.K. Yoo,[15] and J. Zimányi[4,†]

(The NA49 collaboration)

[1] *NIKHEF, Amsterdam, Netherlands.*
[2] *Department of Physics, University of Athens, Athens, Greece.*
[3] *Comenius University, Bratislava, Slovakia.*
[4] *KFKI Research Institute for Particle and Nuclear Physics, Budapest, Hungary.*
[5] *MIT, Cambridge, USA.*
[6] *Henryk Niewodniczanski Institute of Nuclear Physics, Polish Academy of Sciences, Cracow, Poland.*
[7] *Gesellschaft für Schwerionenforschung (GSI), Darmstadt, Germany.*
[8] *Joint Institute for Nuclear Research, Dubna, Russia.*
[9] *Fachbereich Physik der Universität, Frankfurt, Germany.*
[10] *CERN, Geneva, Switzerland.*
[11] *Institute of Physics Świętokrzyska Academy, Kielce, Poland.*
[12] *Fachbereich Physik der Universität, Marburg, Germany.*
[13] *Max-Planck-Institut für Physik, Munich, Germany.*
[14] *Charles University, Faculty of Mathematics and Physics, Institute of Particle and Nuclear Physics, Prague, Czech Republic.*
[15] *Department of Physics, Pusan National University, Pusan, Republic of Korea.*
[16] *Nuclear Physics Laboratory, University of Washington, Seattle, WA, USA.*
[17] *Atomic Physics Department, Sofia University St. Kliment Ohridski, Sofia, Bulgaria.*
[18] *Institute for Nuclear Research and Nuclear Energy, Sofia, Bulgaria.*
[19] *Department of Chemistry, Stony Brook Univ. (SUNYSB), Stony Brook, USA.*
[20] *Institute for Nuclear Studies, Warsaw, Poland.*
[21] *Institute for Experimental Physics, University of Warsaw, Warsaw, Poland.*
[22] *Faculty of Physics, Warsaw University of Technology, Warsaw, Poland.*
[23] *Rudjer Boskovic Institute, Zagreb, Croatia.*

Transverse momentum spectra up to 4.5 GeV/c around midrapidity of $\pi^{\pm}$, p, $\bar{p}$, $K^{\pm}$ in Pb+Pb reactions were measured at $\sqrt{s_{NN}} = 17.3\,\mathrm{GeV}$ by the CERN-NA49 experiment. The nuclear modification factors R_{AA} for $\pi^{\pm}$ and R_{CP} for $\pi^{\pm}, p, \bar{p}, K^{\pm}$ were extracted and are compared to RHIC results at $\sqrt{s_{NN}} = 200\,\mathrm{GeV}$. The modification factor R_{AA} shows a rapid increase with transverse momentum in the covered region. This indicates that the Cronin effect is the dominating effect in our energy range. The modification factor R_{CP}, in which the contribution of the Cronin effect is reduced, shows a saturation well below unity in the $\pi^{\pm}$ channel. The extracted R_{CP} values follow the 200 GeV RHIC results closely in the available transverse momentum range, except for $\pi^{\pm}$ above 2.5 GeV/c transverse momentum. There the measured suppression is smaller than that observed at RHIC.

PACS numbers: 25.75.Dw

*Corresponding author. E-mail address: laszloa@rmki.kfki.hu

†Deceased.

I. INTRODUCTION

One of the most interesting features discovered at RHIC is the suppression of particle production at high transverse momenta in central nucleus-nucleus reactions relative to peripheral ones as well as to p+nucleus and to p+p collisions [1, 2, 3, 4, 5]. This is generally interpreted as a sign of parton energy loss in hot and dense strongly interacting matter.

The aim of the presented analysis is to investigate the energy dependence of these effects via a systematic study of Pb+Pb reactions at top ion-SPS energy, 158A GeV ($\sqrt{s_{NN}} = 17.3$ GeV), with the CERN-NA49 detector. A similar study has been published by the CERN-WA98 collaboration for the π^0 channel [6]. The aim of this paper is to extend their results to all charged particle channels, i.e. $\pi^{\pm}$, p, $\bar{p}$ and $K^{\pm}$.

Invariant yields were extracted as a function of transverse momentum p_T in the range from 0.3 to 4.5 GeV/c in the rapidity interval $-0.3 \leq y \leq 0.7$ (midrapidity), at different collision centralities. The identification of particle types is crucial, because the particle composition of hadron spectra changes rapidly with transverse momentum and differs significantly from that observed at RHIC energies (at SPS energies p production is comparable to the $\pi^{\pm}$ yields already at moderate values of p_T).

The most important results are the nuclear modification factors R_{AA}, which were extracted from the identified charged hadron spectra in Pb+Pb and from the already published p+p pion spectra [7]. It is important to note that the use of reference spectra (e.g. p+p), measured exactly at the same collision energy is necessary, because of the rapid change of the shape of the particle spectra around $\sqrt{s_{NN}} = 17.3$ GeV. A baseline, which is constructed from the existing nearby energy measurements is not sufficient, as discussed in [8].

Besides the in-medium parton energy loss, the R_{AA} quantity can also contain other medium effects, such as the *Cronin effect* [9], a term used for the observation of an increased particle yield at high transverse momentum in p+nucleus compared to the elementary p+p reactions. This effect is believed to be a consequence of multiple scattering of projectile partons (or hadrons) in the nuclei before the particle production process. The Cronin effect could cause a large part of the nuclear modification effects measured by the R_{AA} quantity. For a more sensitive search of the other nuclear effects the R_{CP} (central to peripheral) modification factors were also extracted from the data. If the multiple scattering interpretation of the Cronin effect is correct, its contribution to the R_{CP} ratio is expected to be reduced, as it should already be present in the peripheral baseline.

II. EXPERIMENTAL SETUP

The NA49 detector [10] is a wide-acceptance hadron spectrometer for the study of hadron production in collisions of hadrons or heavy ions at the CERN-SPS. The main components are four large-volume Time Projection Chambers, TPCs, (Fig. 1) which are capable of detecting 80% of some 1500 charged particles created in a central Pb+Pb collision at 158A GeV beam energy. Two chambers, the Vertex TPCs (VTPC-1 and VTPC-2), are located in the magnetic field of two superconducting dipole magnets (1.5 and 1.1 T), while the two others (MTPC-L and MTPC-R) are positioned downstream of the magnets symmetrically to the beam line. The setup is supplemented by two Time of Flight (TOF) detector arrays, which are not used in this analysis, and a set of calorimeters. The NA49 TPCs allow precise measurements of particle momenta p with a resolution of $\sigma(p)/p^2 \cong (0.3 - 7) \cdot 10^{-4}\,(\mathrm{GeV/c})^{-1}$.

Pb foils (typically of 224 mg/cm^2 thickness) are used as target for Pb+Pb collisions, and a liquid hydrogen cylinder (length 20 cm) for p+p interactions. The target is positioned about 80 cm upstream from VTPC-1.

Pb beam particles are identified by means of their charge as seen by a Helium Gas-Čerenkov counter (S2') and proton beam particles by a 2 mm thick scintillator (S2). Both detectors are situated in front of the target. For p beams, interactions in the target are selected by requiring a valid incoming beam particle and no signal from a small scintillation counter (S4) placed on the beam line between the two vertex magnets. For p+p interactions at 158 GeV this counter selects a (trigger) cross section of 28.5 mb out of 31.6 mb of the total inelastic cross section. For Pb-ion beams an interaction trigger is provided by a Helium Gas-Čerenkov counter (S3) directly behind the target. The S3 counter is used to select minimum-bias collisions by requiring a reduction of the Čerenkov signal. Since the Čerenkov signal is proportional to Z^2, this requirement ensures that the Pb projectile has interacted with a minimal constraint on the type of interaction. This setup limits the triggers on non-target interactions to rare beam-gas collisions, the fraction of which proved to be small after cuts, even in the case of peripheral Pb+Pb collisions. The resulting minimum-bias trigger cross section was about 80% of the total inelastic cross section $\sigma_{\mathrm{Inel}} = 7.15$ b.

For Pb+Pb reactions, the centrality of a collision is selected (on-line for central Pb+Pb, off-line for minimum-bias Pb+Pb interactions) by a trigger using information from a downstream calorimeter (VCAL), which measures the energy of the projectile spectator nucleons [11, 12].

III. ANALYSIS

Table I lists the statistics used in the 158A GeV Pb+Pb collision analysis.

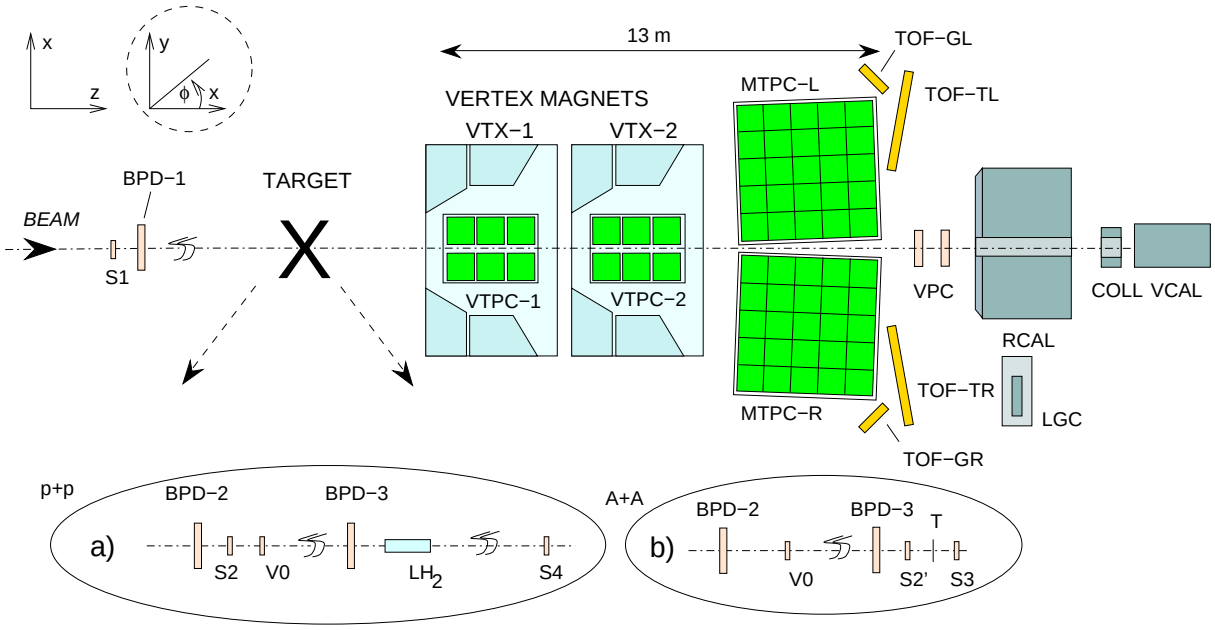

FIG. 1: (Color online) Setup of the CERN-NA49 experiment showing different beam definitions and target arrangements.

Reaction	$\sqrt{s_{NN}}$ [GeV]	Centrality	Number of events
Pb+Pb	17.3	central	830 k
Pb+Pb	17.3	mid-central	1.4 M
Pb+Pb	17.3	peripheral	200 k

TABLE I: The event statistics, used in the analysis.

A. Event Selection

As the target setup of the experiment is not contained in a vacuum pipe, non-target background collisions are also expected to be recorded in the unfiltered event sample. To reduce this contamination, a cut was applied to the reconstructed longitudinal position of the collision point: only those collisions were accepted, which occurred close to the nominal target position. An example plot is shown in Fig. 2 for the case of Pb+Pb reactions, showing the target peak and the small flat non-target contribution, which was used to estimate the remaining background events. The contamination of the peripheral Pb+Pb spectra remains below 5%. For non-peripheral spectra this contamination is zero. The peripheral Pb+Pb spectra are corrected for this effect.

In the case of Pb+Pb reactions, the recorded events were classified by collision centrality, which is correlated to the impact parameter – the transverse distance of the centers of the colliding nuclei at impact. The centrality is determined via the energy measured by the VCAL: the non-interacting (spectator) part of the projectile nucleus travels along the beamline, finally hitting the VCAL's surface, and leaving an energy signal in the apparatus, proportional to the volume of the projectile spectator matter. The higher this energy is, the more peripheral is

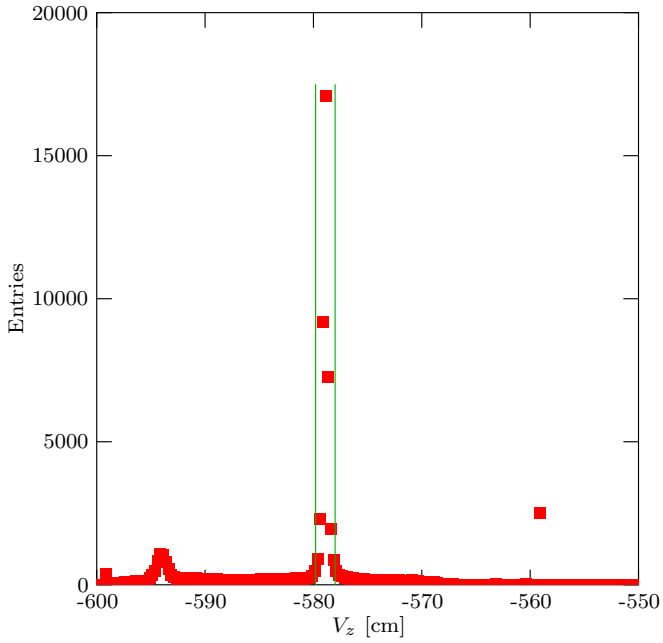

FIG. 2: (Color online) The distribution of the longitudinal coordinate of the reconstructed collision point in minimum-bias Pb+Pb events, together with the cuts. The other peaks correspond to material in the beamline, while the small constant background under the target peak corresponds to beam+gas reactions.

the given reaction. The event centrality is defined by the fraction of total inelastic cross section, i.e. by the running

integral

$$\frac{\sigma(E_{\rm VCAL})}{\sigma_{\rm Inel}} = \frac{1}{\sigma_{\rm Inel}} \int_0^{E_{\rm VCAL}} \frac{{\rm d}\sigma(E'_{\rm VCAL})}{{\rm d}E'_{\rm VCAL}}\, {\rm d}E'_{\rm VCAL},$$

where $\sigma_{\rm Inel}$ is the total inelastic cross section, and $\frac{{\rm d}\sigma}{{\rm d}E_{\rm VCAL}}$ is the differential cross section in $E_{\rm VCAL}$, which is defined by the $E_{\rm VCAL}$ spectrum, normalizing its area to the trigger cross section. The VCAL energy spectrum and event centrality classification is shown in Fig. 3. A relatively large centrality interval was used for the selection of peripheral events in order to gain enough statistics in the particle spectrum analysis.

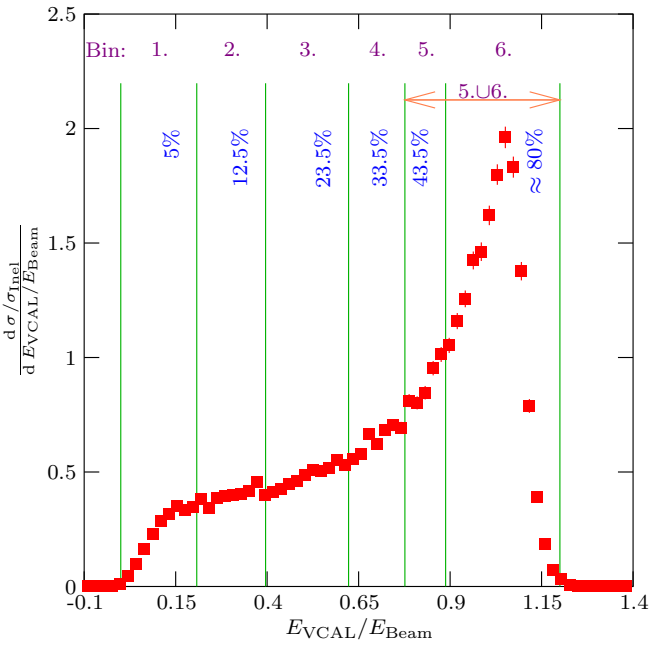

FIG. 3: (Color online) The distribution of the energy deposited in the VCAL by the projectile spectators in Pb+Pb minimum-bias reactions. The centrality intervals selected by fraction of total inelastic cross section are shown by the vertical lines.

Due to the aging of the photomultiplier tubes of the calorimeter, the VCAL response was slowly varying in time in terms of scale offset and amplification. This effect is corrected by a time-dependence calibration procedure, which is based on keeping the correlation of the VCAL energy to the total measured charged multiplicity time-independent (see [13]). The mean values of various collision parameters (number of wounded nucleons, number of binary collisions) for the selected centrality intervals were calculated from the VENUS-4.12 Monte Carlo model [14] which was filtered by the detector simulation. For the non-peripheral region, this was straightforward by applying statistical averaging in the centrality intervals. For the peripheral region, a semi-empiric approach was used, which also takes the trigger bias into account: the VCAL energy distribution for the averaging was taken from the measurement, while the mapping of VCAL energy into collision parameters was taken from VENUS + detector simulation. The procedure is described in [15]. A list of the average values is shown in Table II together with their systematic errors, which were estimated by assuming a 5% uncertainty of the total inelastic cross section, and a 10% uncertainty of the skin thickness of the nuclear density profile. The stated values were also confirmed by the GLISSANDO Monte Carlo model [16].

Bin	Centrality	$\langle N_W \rangle$	$\langle N_{BC} \rangle$
1.	$0-5\%$	357 ± 2	742 ± 18
2.	$5-12.5\%$	288 ± 3	565 ± 18
3.	$12.5-23.5\%$	211 ± 4	379 ± 16
4.	$23.5-33.5\%$	146 ± 5	234 ± 14
5.	$33.5-43.5\%$	87 ± 7 *	120 ± 13 *
6.	$43.5-80\%$	40 ± 4 *	46 ± 5 *
5.∪6.	$33.5-80\%$	56 ± 7 *	70 ± 13 *

TABLE II: The mean values of the number of wounded nucleons and binary collisions in various centrality intervals in Pb+Pb collisions, together with their systematic errors. *: Averages for the full minimum-bias dataset using the semi-empiric method, as discussed in the text.

B. Track Selection

The transverse momentum spectra of particles in heavy-ion collisions are known to decrease rapidly (approximately exponentially) toward higher transverse momenta. Therefore, the background of fake tracks becomes more and more important with increasing p_T, especially for fixed-target experiments, in which the track density is strongly focused in the forward direction, increasing the probability for fake track formation. We apply cuts to minimize the contribution of such artificial tracks. These background tracks consist of discontinuous track candidates, and track candidates whose trajectories pass close to the border of the detector volume. The former kind of tracks mainly arise from erroneous pairing of straight track pieces in MTPC, outside of the magnetic field, to some residual points in the VTPCs. The latter kind of tracks are subject to distortions, as they are likely to have missing or displaced clusters. The corresponding trajectories will have wrong fitted curvature, therefore they should be discarded from the analysis.

The discontinuous track candidates can be easily identified: they are track candidates that (according to their reconstructed charge and momentum) would have left hits in a given TPC (VTPC1, VTPC2, or MTPC), but did not. These tracks were rejected as one source of fake tracks. After this cleaning procedure a 3 dimensional phase space study was performed. Its coordinates are rapidity y, transverse momentum p_T and charge-reflected azimuth ϕ. Charge-reflected azimuth is defined by the azimuth angle of the momentum vector in the transverse plane, whose x-component is multiplied by the charge

sign of the track candidate – the x-direction being perpendicular to the magnetic field and to the beamline. As our detector has an x-reflection symmetry, the use of charge-reflected azimuth enables us to distinguish tracks not crossing the plane defined by the beamline and the magnetic field direction (right-side tracks) from tracks crossing this plane (wrong-side tracks). An example of the track quality distribution as a function of ϕ and p_T is shown in the upper panel of Fig. 4 for a typical rapidity slice. A domain of high quality right-side tracks reveals itself: in this region, the fraction of those tracks with a ratio of the number of measured to number of potential points below 60% is very low. Selection of this region by a 3 dimensional momentum space cut provides a clean track sample. The 3 dimensional momentum space cut is guided by the isosurfaces of the number of potential points, and by the requirement of avoiding efficiency holes, which can be determined from the dropping of the ϕ distribution at fixed (y, p_T) values (the ϕ distribution should be uniform due to the axial symmetry of particle production). The momentum space cut curve is shown by the dotted line in the upper panel of Fig. 4, at given y. The ϕ distribution is shown in the lower panel of Fig. 4 at given (y, p_T), which reveals the efficiency holes to be avoided, and the high track yield excess at the acceptance borders. The dotted arrows indicate the momentum space cut in ϕ, for this particular (y, p_T) slice. The outlined procedure is discussed in detail in [17]. The resulting phase space, which contains the clean track sample, covers the rapidity region $-0.3 \leq y < 0.7$, the transverse momentum region $0\,\mathrm{GeV/c} \leq p_T < 5\,\mathrm{GeV/c}$, and a (y, p_T) dependent ϕ interval. In the following analysis, all distributions will be shown as a function of transverse momentum.

The particle identification was performed via the specific energy loss ($\frac{\mathrm{d}E}{\mathrm{d}x}$) of the particles. In each transverse momentum bin the $\frac{\mathrm{d}E}{\mathrm{d}x}$ spectrum was recorded, and by using the known shape of the response function (see [18, 19]) of the given particle species ($\pi^{\pm}$, $p, \bar{p}$, $K^{\pm}$, $e^{\pm}$), a fit was performed to the $\frac{\mathrm{d}E}{\mathrm{d}x}$ histogram, with the amplitudes of the particle response functions as free parameters. Also other parameters characteristic of the response function shape, such as the most probable value, were kept as free parameters. Thus, their statistical errors are also reflected in the fitted errors of the amplitudes. As our data was limited by statistics at higher p_T, Poisson maximum-likelihood fitting was employed. This approach allows reliable fits even in regions with low statistics (see [20]). An example can be seen in Fig. 5 which demonstrates the $\frac{\mathrm{d}E}{\mathrm{d}x}$ fit procedure for inclusive particle identification in a typical phase space bin. The full procedure is described in [17]. Systematic errors, caused by possible systematic shifts of fit parameters were estimated by calculating the statistical regression matrix from the fitted covariance matrix, and by propagating the systematic errors of the fit parameters (approximately estimated to be about 0.5%) to the fitted yields via this matrix. The resulting systematic errors of yields are estimated to be 4% for K^+, 2% for $\bar{p}$, and 1% for π^+, π^-, p, K^-.

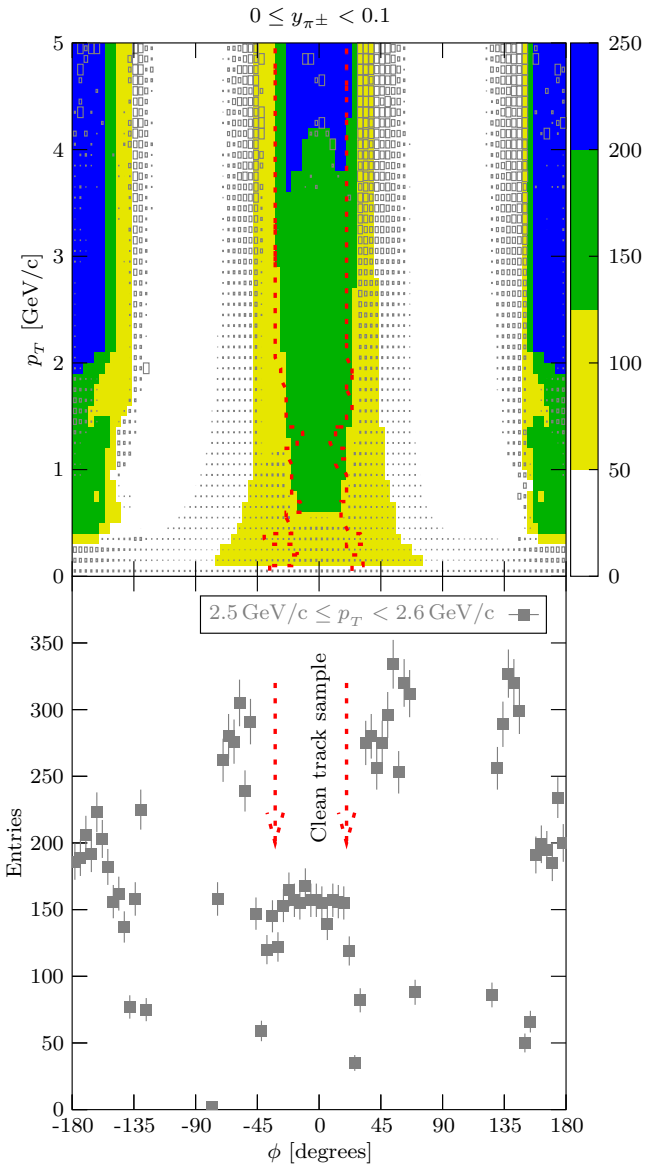

FIG. 4: (Color online) Upper panel: example plot for the momentum space selection in the rapidity slice $0 \leq y < 0.1$, with $\pi^{\pm}$ mass hypothesis. ϕ means charge-reflected azimuth. The size of the boxes indicate the fraction of those track candidates in the given momentum space bin, which have a ratio of number of measured to number of potential points below 60% (i.e. the fraction of those track candidates, which most likely do not correspond to real particle trajectories). The color map indicates the number of potential points as a function of momentum space. As can be seen, the bad track candidates mainly populate the borders of the acceptance. The dotted line shows the momentum space cut, guided by potential point isosurfaces. Lower panel: example plot for the ϕ distribution at $0 \leq y < 0.1$ and $2.5\,\mathrm{GeV/c} \leq p_T < 2.6\,\mathrm{GeV/c}$.

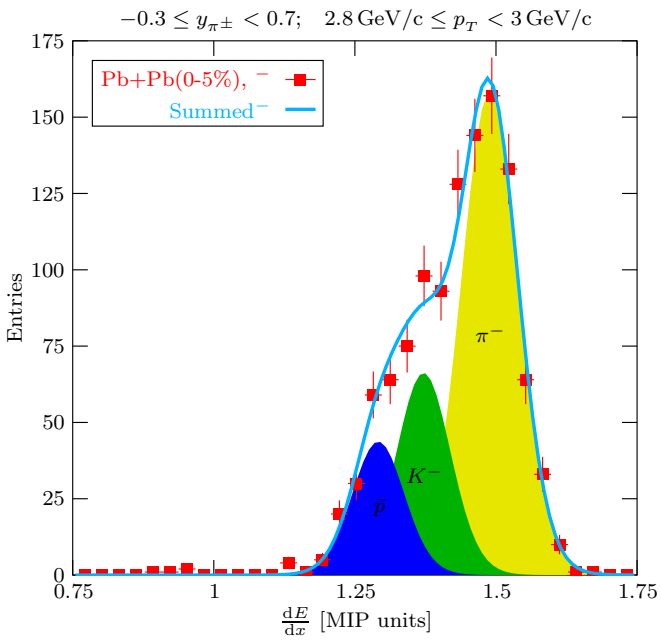

FIG. 5: (Color online) Example plot for the identification of negative particles by specific energy loss fits in central Pb+Pb collisions (0-5%). The parameterization of the response function of each particle species with fixed momentum is known, but the yields (the amplitudes in the summed $\frac{dE}{dx}$ spectrum model) are fit parameters.

C. Corrections

Monte Carlo methods including a GEANT simulation of our detector were used to correct the yields of π^+, π^- and K^+, K^- as well as p and $\bar{p}$ for tracking inefficiencies (below 10%), decay losses (from 20% to 0%), feed-down from weakly decaying particles ($5 - 30\%$), and finally for geometric acceptance. The peripheral particle spectra were also corrected for non-target contamination (5%) by extracting the non-target contribution from pure beam+gas events, and subtracting it (for detailed procedure, see [17]). The yield of fake tracks, after the introduced track cuts, turned out to be negligible. The momentum space resolution was estimated to be better than 1% in the whole region. The momentum scale uncertainty is of the order of 0.1%.

The largest and most sensitive correction is the feed-down correction. The yield of feed-down particles was estimated by using a simulation to determine the conditional probabilities of reconstructing a secondary particle originating from a weakly decaying primary particle as a primary particle. To calculate the feed-down yields as a function of momentum, one has to fold these tables of conditional probabilities with the momentum differentiated yields of the weakly decaying particles. The relevant decay channels are listed in Table III. The yields of the weakly decaying particles K^0_s, $\Lambda, \bar{\Lambda}$ were taken from parameterizations of yields, measured previously in our experiment [21, 22, 23] (K^0_s yield was constructed from average charged Kaon data). The used $\Lambda, \bar{\Lambda}$ yields include the $\Sigma^0 \to \Lambda\gamma$ and the $\bar{\Sigma}^0 \to \bar{\Lambda}\gamma$ contributions, but are feed-down corrected for Ξ ($\bar{\Xi}$) decays. Since the Ξ ($\bar{\Xi}$) yields are generally below 20% of the Λ ($\bar{\Lambda}$) yields, their contribution is neglected in the correction. However, it constitutes a source of systematic errors, that is discussed below. The K^0_s yield does not suffer from feed-down contamination.

K^0_s	$\to \pi^+ \pi^-$	$\leq 5\%$ to $\pi^\pm$
Λ	$\to p \pi^-$	$\leq 30\%$ to p
$\bar{\Lambda}$	$\to \bar{p} \pi^+$	$\leq 30\%$ to $\bar{p}$
Σ^+	$\to p \pi^0$	$\leq 6\%$ to p
Σ^+	$\to n \pi^+$	negligible
Σ^-	$\to n \pi^-$	negligible
$\bar{\Sigma}^-$	$\to \bar{p} \pi^0$	$\leq 6\%$ to $\bar{p}$
$\bar{\Sigma}^-$	$\to \bar{n} \pi^-$	negligible
$\bar{\Sigma}^+$	$\to \bar{n} \pi^+$	negligible

TABLE III: The list of relevant feed-down channels.

For π^+, only the $K^0_s \to \pi^+\pi^-$ channel gives a sizable contribution, while for π^- also the $\Lambda \to p\pi^-$ channel has to be taken into account. All other contributions to the $\pi^\pm$ channels are negligible. For p, the $\Lambda \to p\pi^-$ gives the dominant contribution, and for $\bar{p}$, the $\bar{\Lambda} \to \bar{p}\pi^+$ is dominant. The p and $\bar{p}$ spectra are also contaminated by the decays of Σ^+ and $\bar{\Sigma}^-$. These are taken into account by scaling up the $\Lambda, \bar{\Lambda}$ yields by 20%. This treatment was suggested by the VENUS-4.12 model, which predicts that the relative intensity of the non-Λ contribution to the p feed-down, or the relative intensity of the non-$\bar{\Lambda}$ contribution to the $\bar{p}$ feed-down is approximately constant at 20%. Assuming a 50% systematic uncertainty of this 20% scaling, the contribution to the systematic uncertainty of the $p, \bar{p}$ spectra would be 3%. There is an additional uncertainty of the $\bar{p}$ feed-down correction, which is due to the large errors of the measured $\bar{\Lambda}$ inverse slope parameters. The systematic error, caused by the poor knowledge of the $\bar{\Lambda}$ slopes was estimated by repeating the feed-down calculation using the Λ temperatures, which should provide a reasonable upper bound for the $\bar{\Lambda}$ temperatures. The systematic error, caused by this variation was estimated to be 5%. The calculated feed-down contribution to the $\pi^\pm$ and $p, \bar{p}$ yields in Pb+Pb reactions is depicted in Fig. 6.

The tracking inefficiency was estimated by simulation and reconstruction of embedded particles in real events, i.e. by determining the conditional probability of losing a track of given particle type and momentum, taking the proper track density environment into account. The inefficiency estimates are plotted in Fig. 7. These also include the inefficiency caused by the decay loss for the weakly decaying particles.

The aim of our analysis is to measure the particle yields as a function of p_T at $y = 0$, integrated over $-180° \leq \phi < 180°$. Therefore, the particle spectra have to be corrected for the geometric acceptance. This cor-

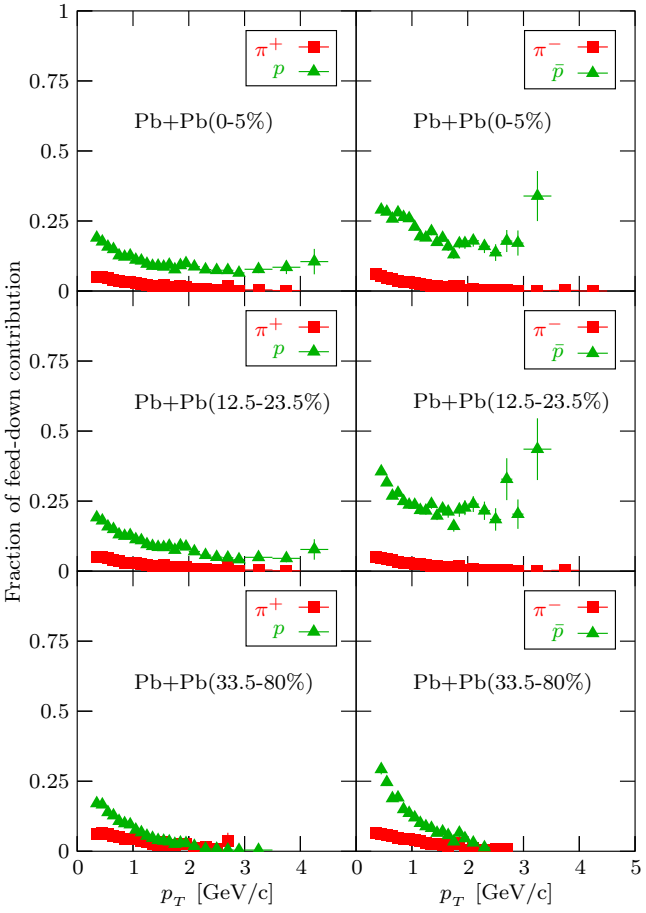

FIG. 6: (Color online) Ratio of the estimated feed-down contribution to the raw measured particle yields. The top, center and bottom row of plots correspond, respectively, to Pb+Pb collisions with centrality ranges of 0-5%, 12.5-23.5% and 33.5-80% of the inelastic cross section (see Table II).

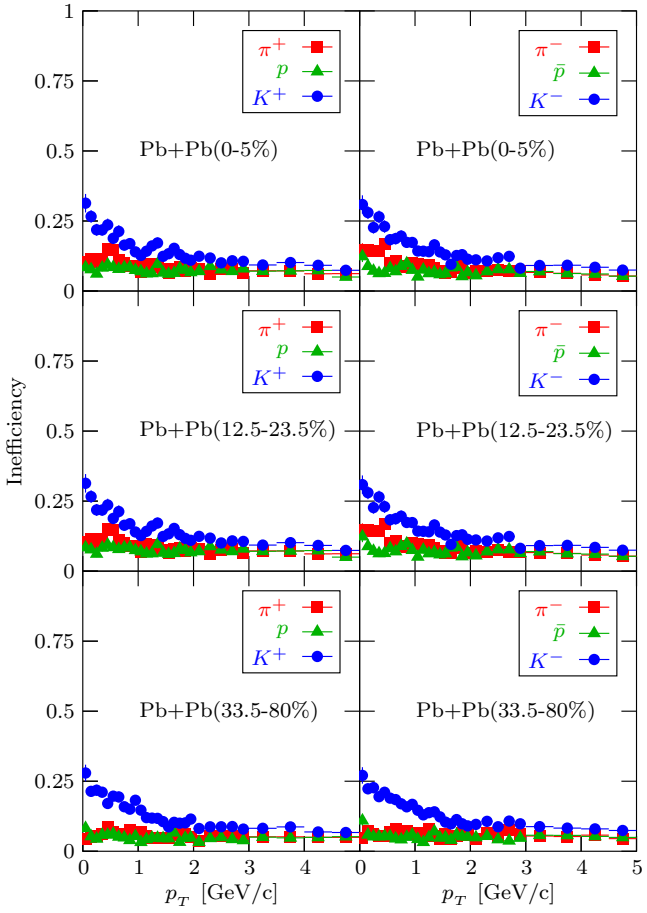

FIG. 7: (Color online) Detection inefficiencies for $\pi^{\pm}$ (squares), $K^{\pm}$ (circles), p and $\bar{p}$ (triangles). The top, center and bottom row of plots correspond to Pb+Pb collisions with centrality ranges of 0-5%, 12.5-23.5% and 33.5-80% of the inelastic cross section (see Table II). The decay loss for $\pi^{\pm}$ and $K^{\pm}$ is included in the inefficiencies.

rection can be performed without simulation, as the accepted momentum space region is defined explicitly by our momentum space cut: only the (y, ϕ) shape of the particle distributions have to be known in each p_T bin. The ϕ distribution is uniform in each (y, p_T) slice due to the axial symmetry of particle production. For the y-dependence we use the fact, that the y spectra around midrapidity are approximately flat in Pb+Pb reactions (see [24]). Therefore, we assume a flat y distribution in $-0.3 \leq y < 0.7$ for the acceptance correction. The systematic error, caused by this approximation has been estimated to be below 2%.

When all the discussed corrections are taken into account, the Pb+Pb particle spectra bear the systematic errors listed in Table IV.

Points which correspond to a fitted amplitude of less than 25 particles or with a statistical error above 30% are not shown. Points below $p_T = 0.3\,\mathrm{GeV/c}$ are not reported at all in order to avoid the $\frac{\mathrm{d}E}{\mathrm{d}x}$ cross-over region.

particle type	$\frac{\mathrm{d}E}{\mathrm{d}x}$	acceptance correction	feed-down yields	feed-down shapes	quadratic sum
π^+	1%	2%			2.2%
π^-	1%	2%			2.2%
p	1%	2%	3%		3.7%
$\bar{p}$	2%	2%	3%	5%	6.5%
K^+	4%	2%			4.5%
K^-	1%	2%			2.2%

TABLE IV: The list of estimated systematic errors and their sources on the $\frac{\mathrm{d}n}{\mathrm{d}p_T}$ values.

IV. RESULTS

A. Charged Hadron Spectra

The resulting hadron spectra are shown in Fig. 8. Preliminary versions, without the discussed corrections have been shown in [25, 26, 27]. The new spectra show

very good agreement with earlier low p_T Pb+Pb results [24, 28]. Also shown in Fig. 8 (lowest panel) are our π^+, π^- spectra measured in p+p interactions [7].

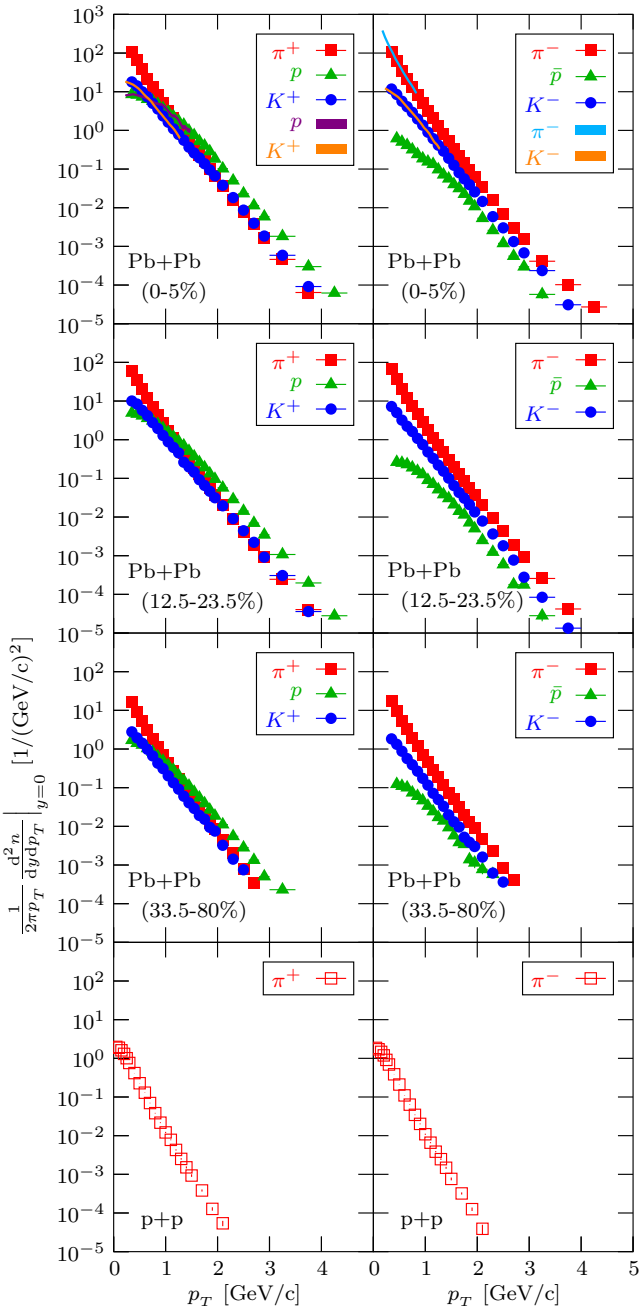

FIG. 8: (Color online) Invariant yields per inelastic collision of $\pi^{\pm}$ (squares), $K^{\pm}$ (circles) and $p, \bar{p}$ (triangles) versus transverse momentum p_T at midrapidity and $\sqrt{s_{NN}} = 17.3$ GeV energy. Results are shown for Pb+Pb collisions with centrality ranges of 0-5% (top row), 12.5-23.5% (second row) and 33.5-80% (third row) of the inelastic cross section (see Table II). Previously published results for central collisions in the lower p_T range [24, 28] are indicated by the bands in the top row. The bottom row shows published NA49 results [7] for π^+ (left) and π^- (right) production in inelastic p+p collisions.

B. Nuclear Modification Factors

The nuclear modification effects are measured by the nuclear modification factors, which are particle yield ratios of two reactions, with appropriate scaling factors. The nuclear modification factors of a reaction $A_1 + A_2$ relative to $A_3 + A_4$ are most generally defined as:

$$R^{BC}_{A_1+A_2/A_3+A_4} = \frac{\langle N_{BC}(A_3+A_4)\rangle}{\langle N_{BC}(A_1+A_2)\rangle} \cdot \frac{\text{yield}(A_1+A_2)}{\text{yield}(A_3+A_4)},$$

and

$$R^{W}_{A_1+A_2/A_3+A_4} = \frac{\langle N_{W}(A_3+A_4)\rangle}{\langle N_{W}(A_1+A_2)\rangle} \cdot \frac{\text{yield}(A_1+A_2)}{\text{yield}(A_3+A_4)}.$$

The ratio $R_{A+A/p+p}$ is in the following abbreviated by the commonly used R_{AA}, while for $R_{p+A/p+p}$ the notation R_{pA} will be used. The scaling factors $\langle N_{BC}\rangle$ and $\langle N_W\rangle$ are the average numbers of binary collisions and of wounded nucleons, respectively, which are calculated according to the Glauber model by Monte Carlo methods which simulate the geometrical configurations. The two different kinds of scaling assumptions are motivated by extreme scenarios of particle production. A pQCD-like particle production scheme would imply a binary collision scaling (particles are produced in binary parton-parton collisions). However, a scenario of a superposition of soft collisions (e.g. particle production via projectile excitation and decay) would rather suggest the scaling of particle production with the number of wounded nucleons, as proposed in e.g. [29] (each collision increases the energy content of the excited nucleon). As the particle production scheme has not been completely determined at SPS energies, especially below 2 GeV/c transverse momentum, both extreme scaling assumptions are examined.

To verify the presence or absence of nuclear effects, we calculate the modification factors R_{AA} and R_{CP} (A+A central/peripheral) for hadrons using our particle spectra at $\sqrt{s_{NN}} = 17.3$ GeV. We compare our results to those obtained at $\sqrt{s_{NN}} = 200$ GeV, measured by the PHENIX experiment at RHIC [2, 4]. As the production of π^+ and π^- is already very similar at our energy, we only show the average of $\pi^{\pm}$ for charged pions. The heavier particle yields ($p, \bar{p}$, K^+, K^-) proved not yet to be symmetric with respect to charge conjugation at our energy and we show them separately. The antiparticle/particle asymmetry of our spectra can be seen in Fig. 9. As p+p is a maximally isospin-asymmetric system, the π^-/π^+ ratio is slightly below one. Pb+Pb is less asymmetric in isospin, thus its π^-/π^+ production ratio is closer to unity. The isospin argument does not hold for the case of K^-/K^+ and $\bar{p}/p$ ratios, which are strongly influenced by the net-baryon density.

The nuclear modification factor R_{AA} is shown in Fig. 10 for the $\pi^{\pm}$ channel at top SPS and RHIC collision energies. The RHIC data are compared to R_{dA} at the same center-of-mass energy, while for the SPS data R_{pA},

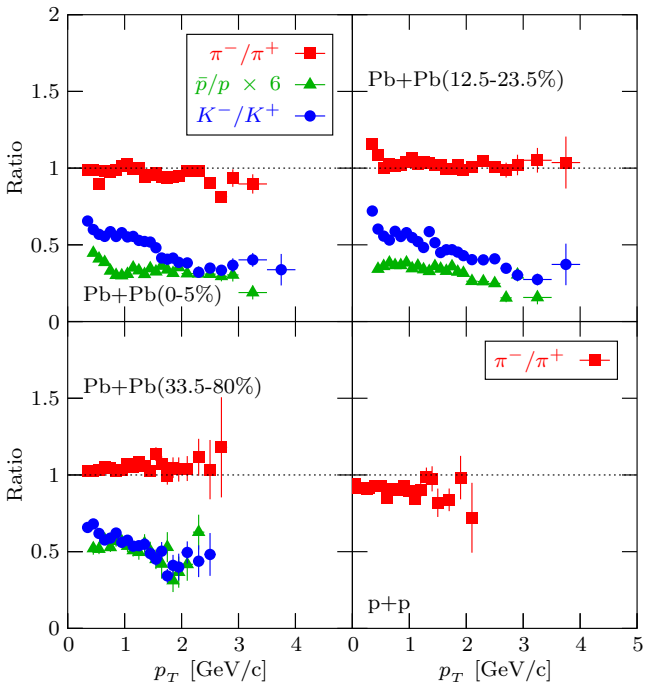

FIG. 9: (Color online) Ratios between antiparticle and particle yields versus transverse momentum p_T at midrapidity and $\sqrt{s_{NN}} = 17.3\,\text{GeV}$ energy. Results are shown for π^-/π^+ (squares), K^-/K^+ (circles) and $\bar{p}/p$ (scaled up by a factor 6, triangles). Plots correspond to Pb+Pb collisions with centrality ranges of 0-5% (top left), 12.5-23.5% (top right) and 33.5-80% (bottom left) of the inelastic cross section (see Table II). Ratios from published NA49 results on π^- and π^+ yields in p+p collisions [7] are plotted in the bottom right panel.

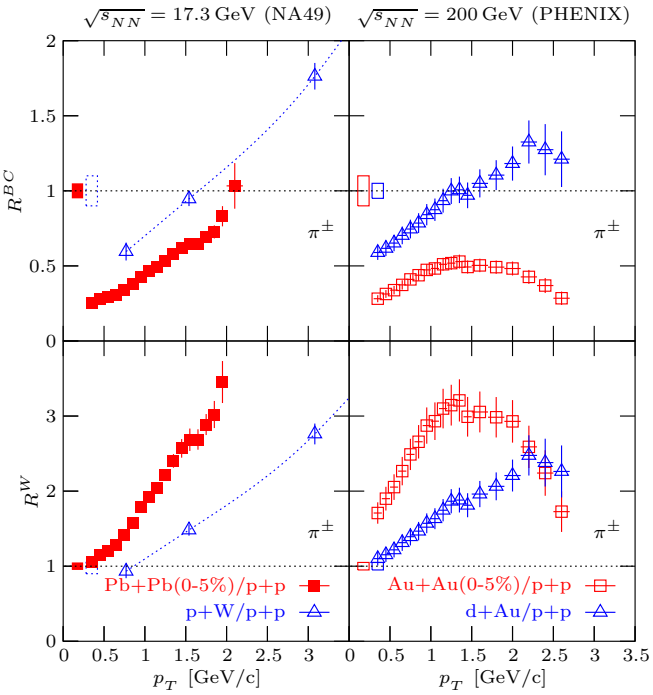

FIG. 10: (Color online) Ratios of charged pion yields at midrapidity in central nucleus+nucleus and inelastic nucleon+nucleon collisions scaled by the number of binary collisions (R^{BC}, top row) and number of wounded nucleons (R^W, bottom row). The left column shows results from NA49 at the SPS ($\sqrt{s_{NN}} = 17.3\,\text{GeV}$) for the ratio of central (0-5%) Pb+Pb collisions to inelastic p+p reactions (filled squares) compared to the ratio of p+W to p+p collisions at $\sqrt{s_{NN}} = 19.4\,\text{GeV}$ [9] (the dotted line is shown to guide the eye). The right column shows measurements from RHIC ($\sqrt{s_{NN}} = 200\,\text{GeV}$) [2, 4] for the ratio of central (0-5%) Au+Au collisions (open squares) and d+Au reactions (open triangles). (The error bars attached to the constant 1 line indicate normalization uncertainty.)

measured at $\sqrt{s_{NN}} = 19.4\,\text{GeV}$ [9], is shown in addition. Since the R_{pA} factors exhibit only a weak energy dependence for $0 \le p_T < 4.5\,\text{GeV/c}$ in the energy range $19.4 \le \sqrt{s_{NN}} \le 27.4\,\text{GeV}$ [9], the comparison to the $\sqrt{s_{NN}} = 17.3\,\text{GeV}$ data is to a certain extent justified. However, the shrinking of the available momentum space region with decreasing collision energy makes this extrapolation in energy somewhat uncertain, as the modification factors are expected to behave singularly close to the momentum space kinematic limit.

The main observations with the binary collision scaling assumption are the following. Both the R_{AA} and the R_{pA} data show a similar low p_T increase at $\sqrt{s_{NN}} = 17.3\,\text{GeV}$ and $\sqrt{s_{NN}} = 200\,\text{GeV}$, up to $p_T \le 1\,\text{GeV/c}$. The R_{pA} ratios rise above 1 at both collision energies with similar slopes, showing an excess of particle yield, which is often called Cronin effect. The 17.3 GeV R_{AA} data keeps rising approximately linearly up to 2 GeV/c, where the statistics of the p+p reference spectrum runs out. In the case of 200 GeV R_{AA} data, the ratio starts to decrease in this region, showing a large suppression both relative to the constant 1 line and to the R_{pA} ratio (the "Cronin baseline"). The evolution of the 17.3 GeV data at $p_T > 2\,\text{GeV/c}$ is not clear, because the available experiments on p+p have no statistics beyond $p_T = 2\,\text{GeV/c}$. In the covered p_T region, the R_{AA} ratio stays below the R_{pA} Cronin baseline also at 17.3 GeV.

When assuming wounded nucleon scaling, there are some differences compared to the above picture. Namely, the modification factors start from one at both energies, and show a rapid increase with similar slopes at the beginning. The R_{pA} ratios stay below the R_{AA} result as opposed to the binary collision case. The 200 GeV R_{AA} data show a tendency of returning to the constant 1 line at $p_T \approx 3\,\text{GeV/c}$.

A widely believed interpretation of the Cronin effect is momentum transfer from the longitudinal degrees of freedom to the transverse degrees of freedom by multiple scattering of partons or hadrons, depending on the picture. However, then this effect must also be present in A+A collisions, and may mask other nuclear effects. On the other hand the nuclear modification factor R_{CP} would not contain most of the contribution of the Cronin

effect. The nuclear modification factor R_{CP} is shown in Fig. 11 for different particle types at top SPS and RHIC collision energies. When assuming binary collision scaling, the $\pi^{\pm}$ ratios show an amazing similarity at the two energies at $p_T \leq 2\,\mathrm{GeV/c}$, above which the 17.3 GeV ratio seems to stay constant (below unity), and the 200 GeV ratio begins to show a large suppression. The p ratios seem to saturate at $p_T \geq 2\,\mathrm{GeV/c}$ at both energies and are almost identical over the whole p_T range. The $\bar{p}$ ratios differ at the two energies. The K^+, K^- results are very similar at the two energies in the common p_T range. In fact, the NA49 $K^{\pm}$ results cover a slightly larger p_T interval than the published PHENIX measurements.

When using wounded nucleon scaling, the modification factors start from one, and show a rapid increase. The $\pi^{\pm}, K^{\pm}$ modification factors show differences between the top SPS and RHIC collision energies. The difference of $\bar{p}$ results is even larger. The p modification factors at top SPS and RHIC energies, however, are quite similar.

In Fig. 12, the available R_{CP} measurements for $\pi^{\pm}$ and π^0 at SPS and RHIC are compared [2, 6, 30]. It is seen that the agreement between the result for $\pi^{\pm}$ from NA49 and π^0 from WA98 for $p_T > 0.8\,\mathrm{GeV/c}$ is quite good within errors. The difference between the PHENIX $\pi^{\pm}$ and π^0 measurements is larger and outside errors.

In conclusion, R_{CP} ratios for identified charged particles scaled by the number of binary collisions are remarkably similar at SPS and RHIC energies. Our present results at the SPS only reach the medium p_T region, where soft production processes and the quark coalescence mechanism [31] may still dominate. It remains to be tested by future experiments, having access to an extended p_T range, whether energy loss of hard scattered partons in dense matter is also a significant process at SPS energies.

V. SUMMARY

Invariant yields of $\pi^{\pm}$, $p, \bar{p}$, $K^{\pm}$ particles were measured in Pb+Pb reactions at $\sqrt{s_{NN}} = 17.3\,\mathrm{GeV}$ collision energy around midrapidity as a function of transverse momentum up to $4.5\,\mathrm{GeV/c}$, with overall systematic errors below $\approx 5\%$. Using these spectra and the previously published $\pi^{\pm}$ yields in p+p collisions, the nuclear modification factor R_{AA} for $\pi^{\pm}$ and R_{CP} for $\pi^{\pm}$, p, $\bar{p}$, $K^{\pm}$ were studied.

The extracted R_{AA} ratio, scaled with the number of binary collisions, shows a rapid rise with transverse momentum in the covered p_T region and does not show the strong suppression observed at RHIC. Interestingly, the R_{CP} ratios for $\pi^{\pm}, K^{\pm}$, and p in the available p_T region stay rather close to the $\sqrt{s_{NN}} = 200\,\mathrm{GeV}$ RHIC results. In fact, R_{CP} ratios for p are almost identical. However, although the $\pi^{\pm}$ ratio stays below one also at the SPS, it shows a much larger suppression at RHIC above 2 GeV/c transverse momentum. When scaled with the number of wounded nucleons, the modification factors R_{AA} and

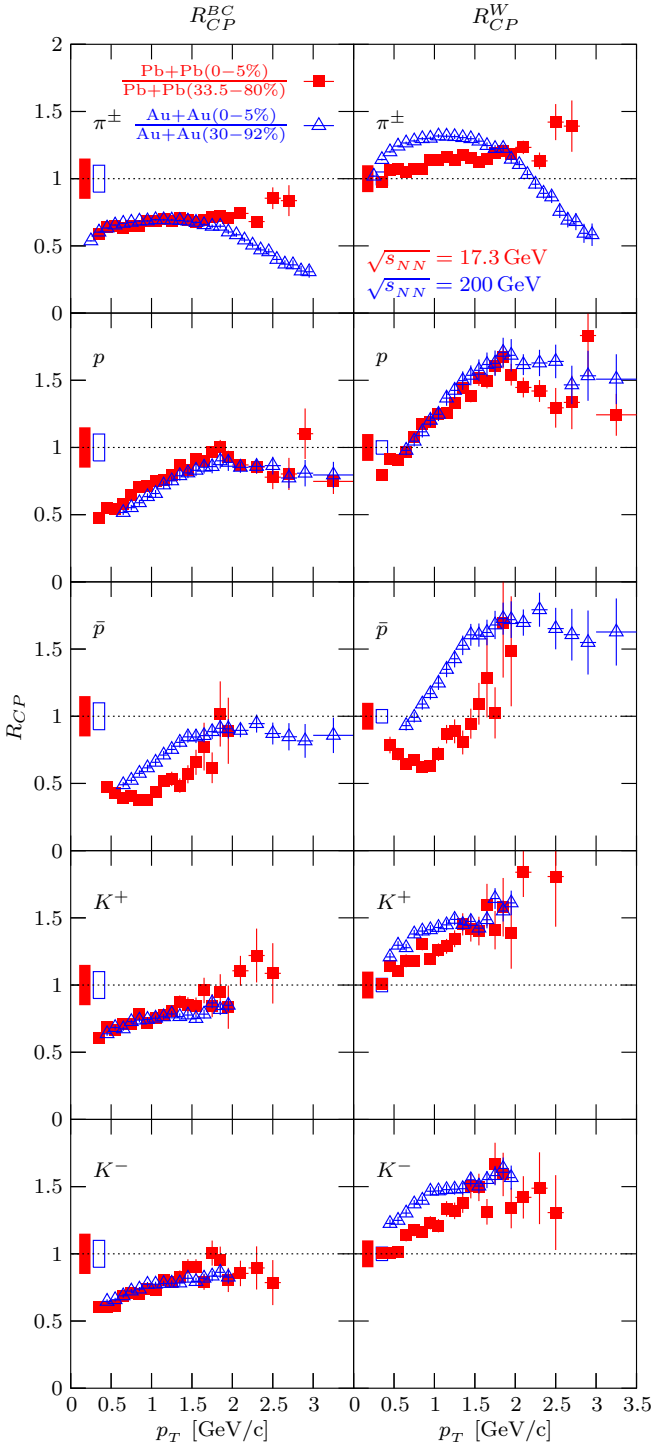

FIG. 11: (Color online) Ratio of yields in central to peripheral Pb+Pb and Au+Au collisions at $\sqrt{s_{NN}} = 17.3\,\mathrm{GeV}$ (squares) and 200 GeV [2] (triangles). Left column shows ratio R_{CP}^{BC} using binary collision scaling, right column shows ratio R_{CP}^{W} using wounded nucleon scaling. Centrality intervals are specified in the legend of the top left panel. (The error bars attached to the constant 1 line indicate normalization uncertainty.)

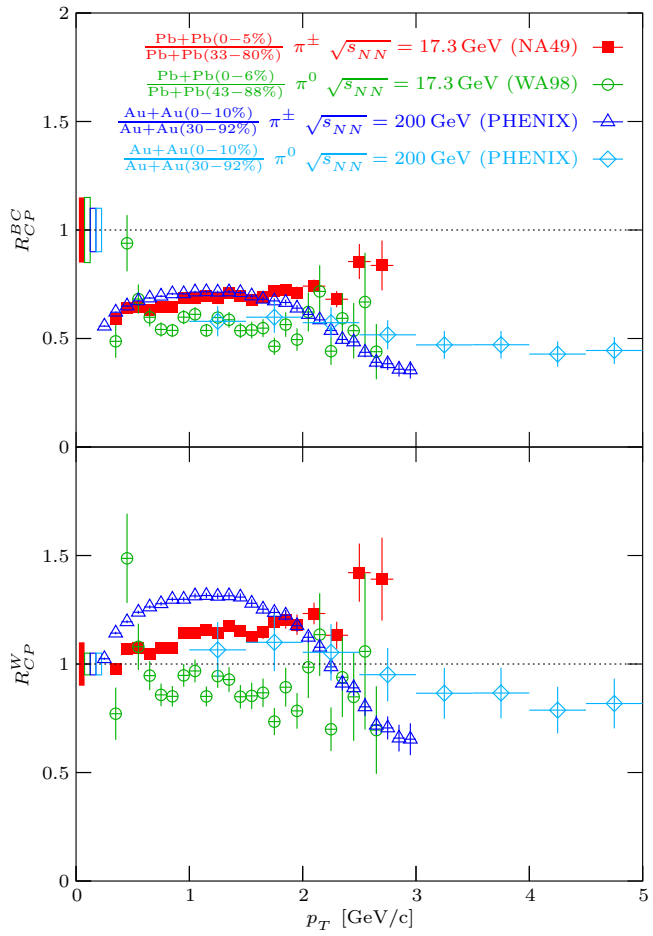

FIG. 12: (Color online) Comparison of nuclear modification factors for $\pi^{\pm}$ and π^0 using binary collision scaling (R_{CP}^{BC}, top) and wounded nucleon scaling (R_{CP}^{W}, bottom). Results at the SPS ($\sqrt{s_{NN}} = 17.3\,\mathrm{GeV}$) in Pb+Pb collisions from NA49 on $\pi^{\pm}$ are shown by squares, from WA98 on π^0 [6] by circles. Measurements from RHIC ($\sqrt{s_{NN}} = 200\,\mathrm{GeV}$) in Au+Au collisions for $\pi^{\pm}$ [2] are plotted as triangles, for π^0 [30] as diamonds. (The error bars attached to the constant 1 line indicate normalization uncertainty.)

R_{CP} start from one and show a rapid rise with p_T, furthermore the R_{pA} ratio stays below R_{AA} in the covered p_T region for both SPS and RHIC collision energies.

The p_T range of our modification factor measurements is limited by the statistics of the p+p and peripheral Pb+Pb collision reference spectra. A recently started second generation experiment, CERN-NA61 [32, 33, 34], will make it possible to extract reference spectra up to higher p_T of 4 GeV/c in p+p and p+Pb collisions matching the p_T range of the currently available central Pb+Pb data. These future measurements will allow a more sensitive test for the presence of high p_T particle suppression at SPS energy.

Acknowledgments

This work was supported by the US Department of Energy Grant DE-FG03-97ER41020/A000, the Bundesministerium fur Bildung und Forschung, Germany, the Virtual Institute VI-146 of Helmholtz Gemeinschaft, Germany, the Polish State Committee for Scientific Research (1 P03B 006 30, 1 P03B 097 29, 1 PO3B 121 29, 1 P03B 127 30), the Hungarian Scientific Research Fund (OTKA 68506), the Polish-German Foundation, the Korea Science & Engineering Foundation (R01-2005-000-10334-0), the Bulgarian National Science Fund (Ph-09/05) and the Croatian Ministry of Science, Education and Sport (Project 098-0982887-2878).

[1] S. S. Adler et al. (the PHENIX Coll.), *Phys. Rev.* **C69** (2004) 034909.
[2] S. S. Adler et al. (the PHENIX Coll.), *Phys. Rev.* **C69** (2004) 034910.
[3] S. S. Adler et al. (the PHENIX Coll.), *Phys. Rev. Lett.* **91** (2003) 072303.
[4] S. S. Adler et al. (the PHENIX Coll.), *Phys. Rev.* **C74** (2006) 024904.
[5] L. Ruan (the STAR Coll.), *J. Phys.* **G31** (2005) s1029.
[6] M. M. Aggarwal et al. (the WA98 Coll.), *Eur. Phys. J.* **C23** (2002) 225; M. M. Aggarwal et al. (the WA98 Coll.) Preprint [arXiv:0708.2630].
[7] C. Alt et al. (the NA49 Coll.), *Eur. Phys. J.* **C45** (2006) 343.
[8] D. d'Enterria, *Phys. Lett.* **B596** (2004) 32.
[9] D. Antreasyan et al., *Phys. Rev.* **D19** (1979) 764.
[10] S. Afanasiev et al. (the NA49 Coll.), *Nucl. Instr. Meth.* **A430** (1999) 210.
[11] C. De Marzo et al., *Nucl. Instr. Meth.* **217** (1983) 405.
[12] H. Appelshäuser et al. (the NA49 Coll.), *Eur. Phys. J.* **A2** (1998) 383.
[13] A. Laszlo, Time-Dependence Calibration of the Veto Calorimeter, NA49 Technical Note (2006) [EDMS:815907]. NA49 Technical Notes are stored on the EDMS repository: [http://edms.cern.ch].
[14] K. Werner, *Phys. Rept.* **232** (1993) 87.
[15] A. Laszlo, Calculating Mean Values of Collision Parameters as a Function of Centrality, NA49 Technical Note (2007) [EDMS:885329].
[16] W. Broniowski, M. Rybczynski, P. Bozek, *Comp. Phys.*

Comm. (2007) submitted [arXiv:0710.5731].
[17] A. Laszlo, High Transverse Momentum Identified Charged Particle Yields in 158 GeV/nucleon Pb+Pb Collisions, NA49 Technical Note (2007) [EDMS:879787].
[18] G. I. Veres, Baryon Momentum Transfer in Hadronic and Nuclear Collisions at the CERN NA49 Experiment, Ph.D. dissertation (2001) Eötvös University, Budapest [EDMS:818513].
[19] D. Varga, Study of Inclusive and Correlated Particle Production in Elementary Hadronic Interactions, Ph.D. dissertation (2003) Eötvös University, Budapest [EDMS:900941].
[20] S. Baker, R. D. Cousins, *Nucl. Instr. Meth.* **A221** (1984) 437.
[21] J. Bächler et al. (the NA49 Coll.), *Nucl. Phys.* **A661** (1999) 45.
[22] C. Blume et al. (the NA49 Coll.), *J. Phys.* **G34** (2007) s951.
[23] A compilation of particle production parameters, measured at CERN-NA49 [http://na49info.web.cern.ch/na49info/na49/Archives/Data/NA49NumericalResults].
[24] S. Afanasiev et al. (the NA49 Coll.), *Phys. Rev.* **C66** (2002) 054902.
[25] A. Laszlo, T. Schuster (for the NA49 Coll.), *Nucl. Phys.* **A774** (2006) 473.
[26] T. Schuster, A. Laszlo (for the NA49 Coll.), *J. Phys.* **G32** (2006) s479.
[27] A. Laszlo, Z. Fodor, G. Vesztergombi (for the NA49 Coll.), *Int. J. Mod. Phys.* **E16** (2007) 2516.
[28] T. Anticic et al. (the NA49 Coll.), *Phys. Rev.* **C69** (2004) 024902.
[29] A. Bialas, M. Bleszynski, W. Czyz, *Nucl. Phys.* **B111** (1976) 461; A. Bialas, W. Czyz, *Acta Phys. Polon.* **B36** (2005) 905.
[30] S. S. Adler et al. (the PHENIX Coll.), *Phys. Rev. Lett.* **91** (2003) 072301.
[31] V. Greco et al., *Phys. Rev. Lett.* **90** (2003) 202302; R. J. Fries et al., *Phys. Rev. Lett.* **90** (2003) 202303; R. C. Hwa, C. B. Yang, *Phys. Rev.* **C70** (2004) 024904.
[32] N. Antoniou et al. (the NA61 Coll.), Study of Hadron Production in Collisions of Protons and Nuclei at the CERN SPS, NA49-future Letter of Intent (2006) [CDS:CERN-SPSC-2006-001, SPSC-I-235]. CERN documents are stored on the CDS repository: [http://cds.cern.ch].
[33] N. Antoniou et al. (the NA61 Coll.), Study of Hadron Production in Hadron-Nucleus and Nucleus-Nucleus Collisions at the CERN SPS, NA49-future Proposal (2006) [CDS:CERN-SPSC-2006-034, SPSC-P-330].
[34] N. Antoniou et al. (the NA61 Coll.), Additional Information Requested in the Proposal Review Process, Addendum to the NA49-future Proposal (2007) [CDS:CERN-SPSC-2007-004, SPSC-P-330].